

# Detecting small anatomical change with 3D serial MR subtraction images

M. Holden<sup>a</sup>, E. R. E. Denton<sup>b</sup>, J. M. Jarosz<sup>b</sup>, T. C. S. Cox<sup>c</sup>, C. Studholme<sup>d</sup>, D. J. Hawkes<sup>a</sup>  
and D. L. G. Hill<sup>a</sup>

<sup>a</sup>Radiological Sciences, GKT Medical School, Guy's Hospital, London SE1 9RT, UK

<sup>b</sup>Radiology, King's College Hospital, Denmark Hill, London, UK

<sup>c</sup>Institute of Neurology, UCL, Queen's Square, London, UK

<sup>d</sup>Diagnostic Radiology, Yale School of Medicine, New Haven, CT, USA

## ABSTRACT

Spoiled gradient echo volume MR scans were obtained from 5 growth hormone (GH) patients and 6 normal controls. The patients were scanned before treatment and after 3 and 6 months of GH therapy. The controls were scanned at similar intervals. A calibration phantom was scanned on the same day as each subject. The phantom images were registered with a 9 degree of freedom algorithm to measure scaling errors due to changes in scanner calibration. The second and third images were each registered with a 6 degree of freedom algorithm to the first (baseline) image by maximising normalised mutual information, and transformed, with and without scaling error correction, using sinc interpolation. Each registered and transformed image had the baseline image subtracted to generate a difference image. Two neuro-radiologists were trained to detect structural change with difference images containing synthetic misregistration and scale changes. They carried out a blinded assessment of anatomical change for the unregistered; aligned and subtracted; and scale corrected, aligned and subtracted images. The results show a significant improvement in the detection of structural change and inter-observer agreement when aligned and subtracted images were used instead of unregistered ones. The structural change corresponded to an increase in brain:CSF ratio.

**Keywords:** serial MR, brain, growth hormone, subtraction, visual assessment, anatomical change, registration

## 1. INTRODUCTION

The detection of small scale anatomical brain changes is useful for the early evaluation of therapy, as well as for disease diagnosis and monitoring. Subtraction images derived from automatic rigid body alignment of serial MR volume scans can be used to detect subtle change that is not detectable by examination of the original images.<sup>1</sup> Our central aim was to test this hypothesis by investigating whether small scale anatomical change, not observed by conventional radiological examination, could be found by the assessment of subtraction images. We chose to study a group of growth hormone (GH) deficient adult patients undergoing therapy. The benefits of GH therapy are well established for children, but for adults the effects are much less well known. There are well documented changes in body composition, an increase in lean body mass and a corresponding decrease in fat mass.<sup>2,3</sup> GH deficiency leads to impaired psychological well being and capacity which improves following GH replacement therapy.<sup>4,5</sup> Increases in insulin-like growth factor concentration and glucose metabolism in the CSF have been demonstrated.<sup>6,7</sup> This suggests that GH therapy has a direct effect on the central nervous system which may result in structural change. There has been no previous systematic study aimed at determining whether there are any significant changes or how these compare with those for normal volunteers. Conventional examination of MR images of GH patients have not shown any substantial brain change, so any changes that may occur are likely to be small scale. Our work aims at making a systematic comparison of structural change, assessed visually by radiologists, using conventionally unregistered images and also using subtraction images, derived from serial acquisitions. All assessments were done by two independent radiologists who were unaware of the subject and image processing method. Because the radiologists had no previous experience with difference images we trained them to recognise volume change and rigid body misregistration from specially constructed synthetic images. A fundamental difficulty with comparing

---

Further author information: (Send correspondence to D. L. G. Hill)  
D. L. G. Hill: E-mail: Derek.Hill@kcl.ac.uk

serial acquisitions is the effects scaling errors caused by the MR gradient mis-calibration.<sup>1,8,9</sup> These errors result in changes in voxel dimensions of one serial image relative to the other and can be confused with actual anatomical change. To correct for such changes our imaging protocol includes a scan of a calibration phantom that allows us to measure and correct these. We have produced a set of scale corrected difference images as well as the uncorrected ones and assessed all three sets for structural change.

## 2. MATERIALS AND METHOD

### 2.1. Subjects and Imaging

Five GH deficient patients and 6 normal healthy volunteers (controls) were scanned 3 times at 3 monthly intervals. Therapy was administered to the GH patients following the first (baseline) scan and continued through the second and third (repeat) scans. For all subjects the full brain, including cerebellum and brain stem, was imaged at high resolution with a 3D fast spoiled GRE sequence to provide good grey/white matter contrast. All acquisitions were with a 1T Siemens Impact Expert using a 3D Flash spoiled gradient echo sequence: 256x192x169mm FOV; 256x256x94, 1x1x1.8mm voxels; axial slices; 20/6/2/60 (TR/TE/NEX/flip); the readout gradient was in the posterior/anterior direction with a field strength of 4.587 mT/m. On each day that a subject was scanned a calibration phantom was also scanned, once with its axes parallel to the gradient field and once with a small angle in the sagittal plane (see Figure 2).

### 2.2. Determining changes in Patient Orientation

To correct for gross changes in the patient position the repeat images were registered to the coordinate frame of the baseline image. The brain is a relatively rigid structure, but other tissue, particularly the scalp is subject to deformation.<sup>10</sup> So as to exclude the influence of deformable tissue that does not conform to the rigid body assumption the baseline images were segmented to exclude all voxels corresponding to extra-dural tissue. This was done manually by a radiologist with the Analyze package (Mayo clinic, Rochester, MN). A 6 degree of freedom (rigid body) registration algorithm based on the overlap invariant normalised mutual information similarity measure<sup>11,12</sup> was used to estimate the spatial transformation between the repeat and baseline images. This algorithm uses multi-resolution search strategy to quickly find an optimal solution. For these experiments we used 5 levels. The first (finest) level was constructed by trilinear interpolation to an isotropic voxel dimension of  $1 \times 1 \times 1$  mm. The next finest level was resampled with a Gaussian low pass filter  $2 \times 2 \times 2$  mm and subsequent ones were derived from this by calculating the 8 neighbour mean voxel intensity from the previous level. The algorithm proceeds by applying a spatial transformation (tri-linear interpolation) to one image ( $I_2$ , repeat) and calculating the match similarity with the target image ( $I_1$ , baseline) (see Figure 1). The algorithm tests for a better match  $+/-$  the current search interval in each of the 6 degrees of freedom relative to the current transformation. The search interval is numerically the same in each of the 6 degrees of freedom. Translations are in mm and rotations in degrees. This initial interval is 8 mm or degrees which is reduced by a factor of  $\sqrt{2}$  to a final one of  $2^{-5} = 0.03125$  mm or degrees.

### 2.3. Measuring Spatial Scale changes

The instability of the MR scanner's gradient fields,  $G_x$ ,  $G_y$ ,  $G_z$ , over time intervals of many months, lead to scaling errors that result in changes in voxel dimensions between serial acquisitions.<sup>1,9</sup> Over intervals of many minutes the fields are stable, so a scan of a calibration phantom taken on the same day as a subject provides a reliable record of voxel size. We can measure the voxel dimensions of the image of the calibration phantom by registering it with a 9 degree of freedom algorithm. For the absolute voxel size we register to a fixed gold standard (as provided by a model). For the relative change in size we register to another serial phantom image.<sup>13</sup> Figure 2 shows an image of the model, an axial and an angled acquisition of the calibration phantom. For each study subject we measured relative change between the repeat images and the baseline image by registering the corresponding axial phantom scans and extracting the scale factors,  $s_x$ ,  $s_y$ ,  $s_z$ . It is common practice, when imaging the brain, to rotate the  $G_y$ ,  $G_z$  gradients by a small angle ( $\theta < 20^\circ$ , see Figure 3) so that the brain is orientated in the centre of the FOV. We can make a small correction to the scaling factors to allow for this by applying a corresponding rotation to  $s_y$ ,  $s_z$ .

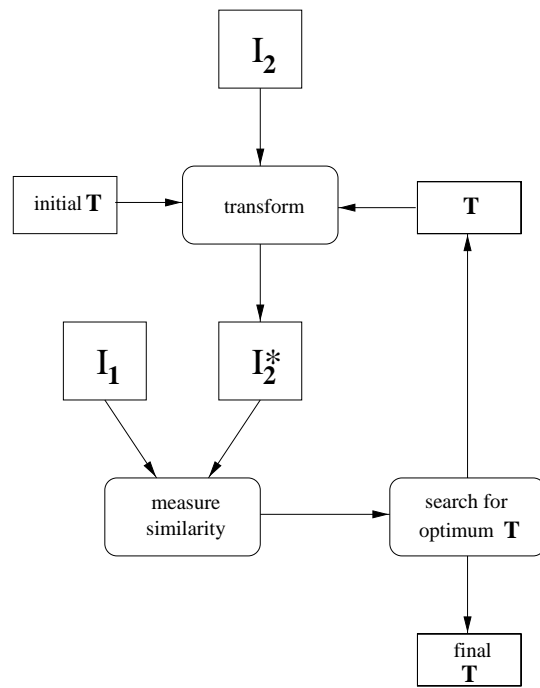


**Figure 1.** Schematic representation of flow of control of registration algorithm for a single resolution level.  $I_1$  (baseline image),  $I_2$  (repeat image),  $I_2^*$  (repeat image spatially transformed by  $\mathbf{T}$ ). The initial transformation  $\mathbf{T}$  is iteratively modified to maximise the similarity of  $I_1$  and  $I_2^*$ .

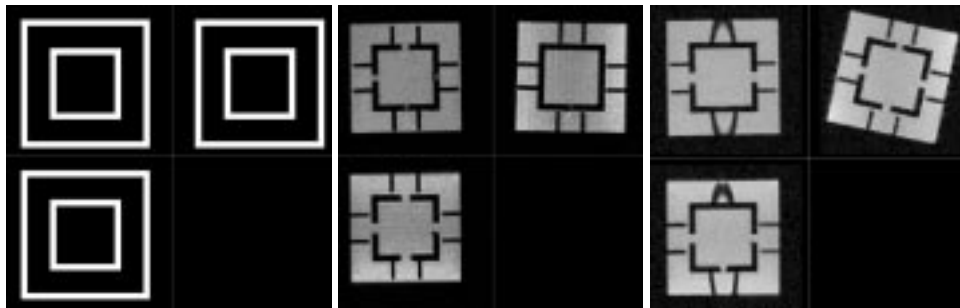


**Figure 2.** Computer model of calibration phantom (left), axial MR scan of calibration phantom (middle), angled MR scan of calibration phantom (right). Shown for each are axial plane (top left) sagittal (top right) and coronal (bottom left).

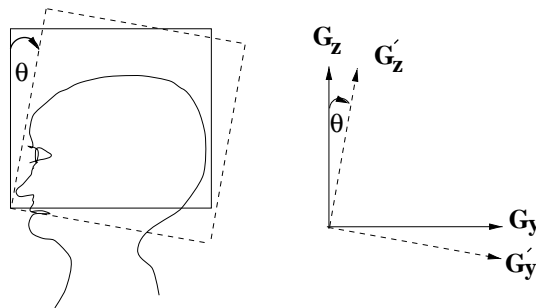


**Figure 3.** Diagram to illustrate how angulation rotates the gradient fields in the sagittal plane by an angle  $\theta$ .

## 2.4. Alignment of Repeat Scans

For band-limited images with regularly spaced sample points a sinc function ( $\frac{\sin(x)}{x}$ ) is theoretically ideal,<sup>14</sup> however, in practice, it must be truncated with a windowing function which degrades its Fourier domain properties. We have decided to use a sinc kernel (radius 6 zero-crossings) truncated with a Hanning window.<sup>10</sup> The voxel sizes of the repeat images were first corrected by multiplying them with the scale factors (measured with the 9 degree of freedom algorithm). Then the repeat images were transformed into the coordinate frame of the baseline image with the rigid body transformations found by the 6 degree of freedom registration algorithm. Sinc interpolation is the most computationally expensive procedure, an order of magnitude slower than the registration, typically taking 5 hours on a 300 MHz Sun Ultra 10.

## 2.5. Intensity Distortion and Subtraction

There are several possible reasons why the voxel intensity in a perfectly aligned repeat image may differ from that of the baseline image: (1) image noise; (2) patient motion during acquisition; (3) RF inhomogeneity; (4) wraparound; (5) changes in the amplifier gain; (6) anatomical change. The parameters of the Rician noise distribution should not change either between voxel locations or over time so image noise should affect corresponding voxels equally. Patient motion artefacts are inevitable. Even if the subject remains perfectly still during the acquisition there will always be local motion artefacts due to blood and CSF flow. RF inhomogeneity is spatially dependent. In our images it is most noticeable at the lower parts of the image near the brain stem and cerebellum. Wraparound is due to signals generated outside the FOV being wrapped into it. For our images the lower part of the head is wrapped into the upper slices. RF inhomogeneity and wraparound will both be dependent on patient position within the scanner. Amplifier gain may vary over time and depend on the orientation of the head in the scanner. For GH patients large changes in body composition are more likely in tissue with a high fat content, i.e. the scalp. Changes in the brain are likely to be small. Table 1 shows the mean voxel intensity over the sub-dural brain region (ROI) for all 3 scans of each of the 11 subjects. So that measurements could be made for the corresponding voxels of the repeat scans the mask defining the ROI in the space of baseline image was transformed to the coordinate frame of the repeat images. This was done by using the inverse of the transformation estimates found by registration. Of course the transformation estimates will have some small error, but this is likely to be less than the error that would arise from the inconsistency individual segmentations of the repeat images. The largest change in mean intensity was -4.77 grey levels for subject 6. Figure 4 shows how the mean intensity of axial slices varies as a function of z for the baseline

**Table 1.** Mean (stdev) intensity of ROI (defined in baseline image)

Subject	Scan 1	Scan 2	Scan 3	2-1	3-1
1	63.45 (28.72)	64.65 (32.83)	61.94 (31.46)	1.20	-1.51
2	62.50 (21.57)	59.56 (26.64)	58.20 (26.10)	-2.94	-4.30
3	64.16 (26.49)	64.64 (30.90)	60.39 (27.64)	0.48	-3.77
4	63.46 (22.27)	62.58 (27.83)	62.87 (26.74)	-0.88	-0.59
5	60.95 (20.18)	60.96 (24.58)	58.07 (21.76)	0.01	-2.88
6	61.29 (24.03)	59.35 (26.25)	56.52 (26.63)	-1.94	-4.77
7	61.44 (23.31)	59.18 (29.69)	58.23 (28.80)	-2.26	-3.21
8	59.62 (28.25)	57.48 (30.85)	56.94 (28.89)	-2.14	-2.68
9	55.71 (22.45)	58.05 (24.30)	55.09 (23.38)	2.34	-0.62
10	56.81 (21.99)	57.83 (26.99)	58.81 (28.10)	1.02	2.00
11	61.30 (22.53)	59.94 (25.28)	58.59 (25.86)	-1.36	-2.71

image and repeat scans of subject 6. The change in mean intensity are much greater between scans 1 and 3 than between 1 and 2 and these differences were largest for slices 0-20 (cerebellum and brain stem) and 65-72 (upper part of brain). There is a strong z-dependence in these regions. The difference in the lower region is probably due to RF inhomogeneity. This suggests that a simple method such as correcting for intensity scaling by dividing both images by the mean of intensity of brain voxel<sup>8,15</sup> would lead to error. A better strategy would probably be to correct for

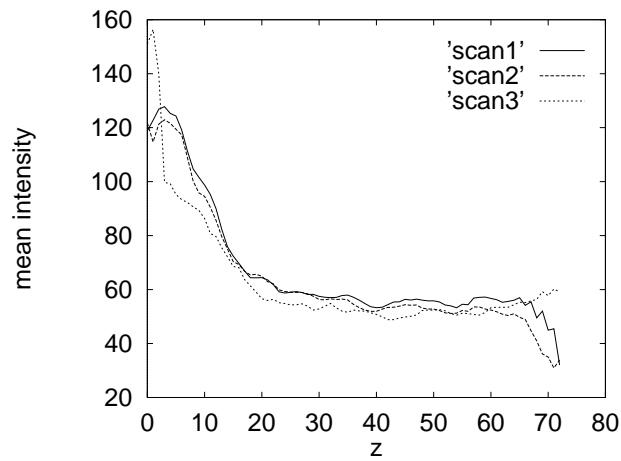


**Figure 4.** Graph of the mean intensity of axial slices in the ROI for three serial scans of subject 6 plotted as a function of  $z$  (slice number). Low  $z$  is caudal, high  $z$  is cranial.

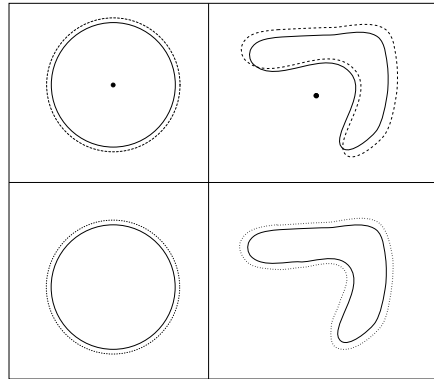


**Figure 5.** Schematic illustration of the distinction between uniform scale change (top row) and anatomical change (bottom). For a circularly symmetric structure (left) the boundary is uniform in both cases so there is always a possible ambiguity, whereas for a non-symmetric structure (right) the boundary is irregular for scale change and regular for anatomical change. The central dot in the upper row indicates the scaling origin.

the spatial dependence of intensity distortion.<sup>16,17</sup> We chose not to do any intensity correction prior to subtraction for this study.

## 2.6. Interpretation of Difference Images

The pattern of signals in the difference image allows the type of change that has occurred between the acquisitions to be distinguished. A pattern without spatial correlation and subject related structure indicates that there has not been any change. Symmetric bright/dark patterns indicate misregistration (see Figure 7). A band of the same intensity indicates either a scale change or anatomical change. The latter case is the most difficult to distinguish, particularly if scale changes are non-uniform. Scale change is global throughout the image, whereas anatomical change occurs locally within a structure and is likely to result in a uniform boundary change. Figure 5 illustrates how anatomical change can be distinguished from uniform scale change.

Neither radiologist had much previous experience of interpreting difference images so we decided to train them to recognise the following cases: (1) misregistration (3 translations and 3 rotations); (2) misregistration in the  $z$  (inferior-superior) direction; (3) uniform spatial scaling increase and decrease. For training data we used a pair of images of another volunteer. These were acquired consecutively so as to exclude the possibility of anatomical change occurring between them. For (1) we simulated typical misregistration that might occur in our data both in terms of

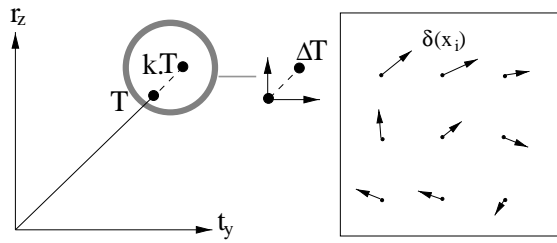


**Figure 6.** Schematic illustration (in 2D) of how small amounts of misregistration were generated (left).  $\mathbf{T}$  is the transformation for perfect alignment.  $k$  is a constant close to unity.  $k\mathbf{T}$  is the transformation applied which results in a small residual misregistration,  $\Delta\mathbf{T}$ , relative to  $\mathbf{T}$ . The displacement of voxel locations relative to perfect alignment,  $\mathbf{T}$ , is shown in the right panel.  $\delta(\mathbf{x}_i)$  is the displacement of  $i$ th voxel location  $\mathbf{x}_i$ , and varies across the FOV unless  $\Delta\mathbf{T}$  is a pure translation.

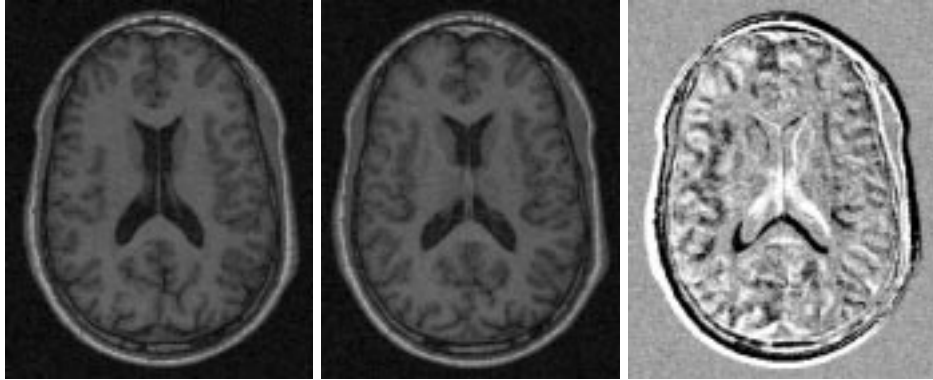


**Figure 7.** Mid axial slice of baseline image (left) unaligned repeat image (middle) and difference image (repeat - baseline).

both magnitude (sub-voxel) and direction (6 degrees of freedom). This was derived by scaling up the transformation found by registration, i.e. multiplying each of the six coordinates (corresponding to each of the six degrees of freedom) by a factor that was slightly less than unity (see Figure 6). Of course there will always be small errors in the original transformation,  $\mathbf{T}$ , because of imperfections of the registration algorithm and discretisation of its search space, but the probability of this error corresponding to the residual misregistration is negligibly small. We chose to measure misregistration arising from  $\Delta T$  by calculating the mean shift in voxel location,  $dp$ , for those voxels corresponding to the baseline ROI ( $I_0$ ). This can be calculated by summing the magnitude of the displacement of each voxel in the ROI,  $|\delta(\mathbf{x}(i))|$ , and dividing by the number of voxels in the ROI,  $N$ , i.e.

$$dp = \frac{1}{N} \sum_{\forall i \in I_0} |\delta(\mathbf{x}(i))| \quad (1)$$

Figures 7, 8, 9 illustrate the impact that misregistration has on the difference image. Figure 7 shows gross misregistration artefacts that occur when the images are subtracted without alignment. Figure 8 shows that accurate alignment results in a difference image with a noise-like signal. Figure 9 shows the effect of adding small (sub-voxel) amounts of misregistration. The most noticeable changes to the difference image are near the lateral ventricle walls where there is most contrast between white matter (high intensity) and CSF (low intensity). For (2) we chose a pure  $z$  translation to demonstrate the possible ambiguity caused by a shift through the viewing plane of the difference image. Figure 10 illustrates how difference signals may be generated in the axial plane by a high contrast convex surface (eg a ventricle wall) moving through it. To illustrate the effects of scale changes we produced example difference images where the repeat image had been uniformly scaled up and down by 1 % prior to subtraction (see Figure 11). This was done by multiplying the voxel dimensions by a scalar and then transforming with the sinc kernel. Figure 12 shows these changes affect the difference image. Within the sub-dural brain region the most noticeable

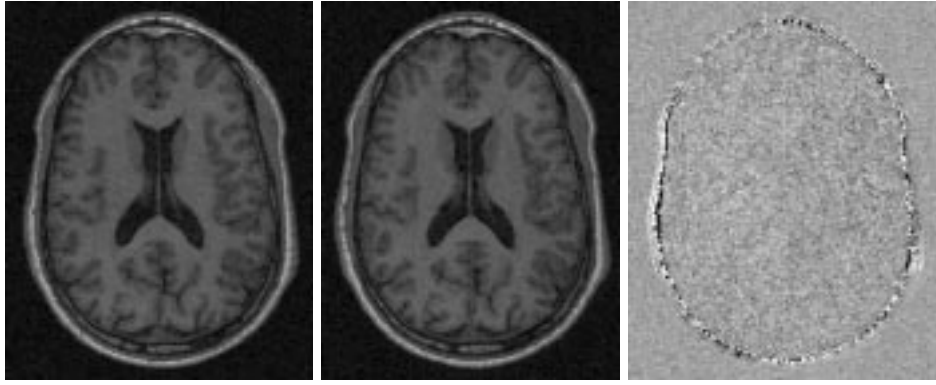


**Figure 8.** Mid axial slice of baseline image (left) aligned repeat image (middle) and difference image (repeat - baseline)

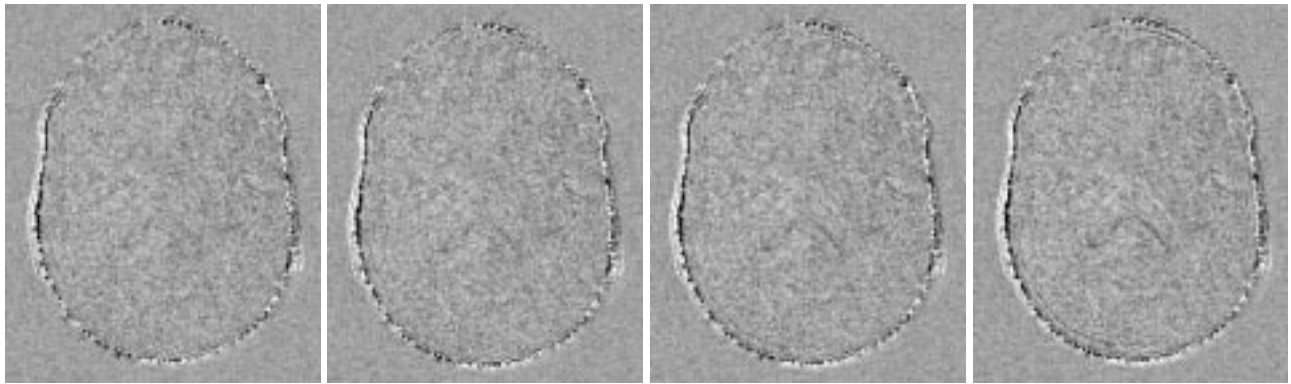


**Figure 9.** Difference images from the same images as the above, but with successively larger amounts of added misregistration. Mean voxel shift is  $100\mu m$  (left) increasing by  $100\mu m$  increments to  $400\mu m$  (right). Notice how the shading on the ventricle increases with added misregistration.

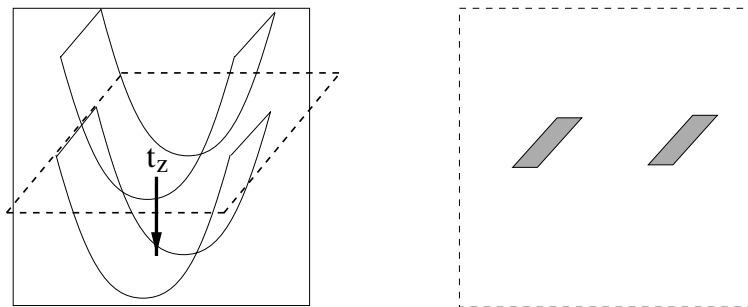


**Figure 10.** Translation ( $t_z$ ) of a high contrast convex surface viewed from the coronal plane (left panel). The axial plane is indicated by dashed lines and the corresponding signals generated in the axial plane of the difference image (right panel)

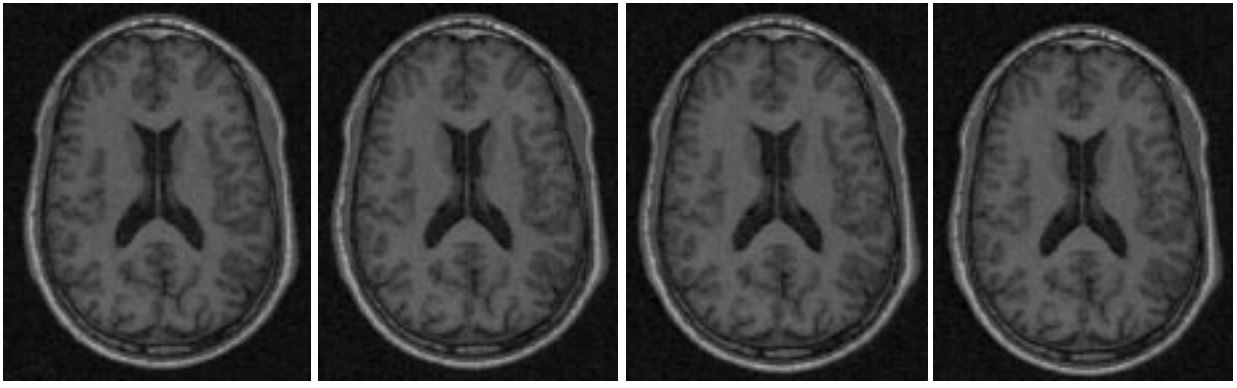


**Figure 11.** Examples of uniform scale change. Mid axial slices of: baseline (left), aligned repeat, repeat scaled by +1 %, -1 % (right).

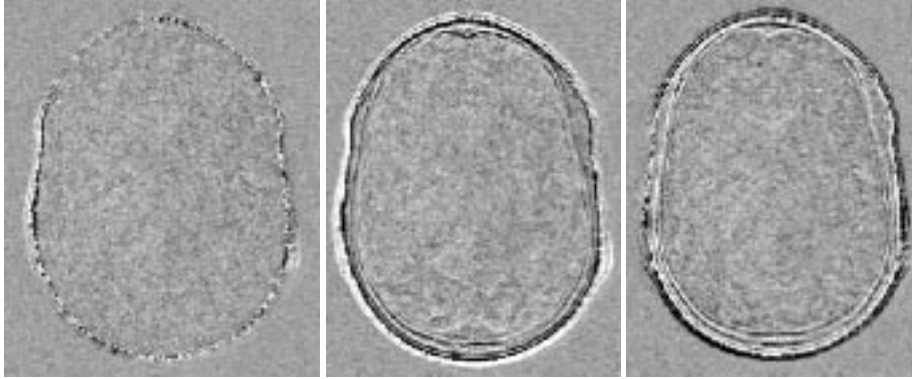


**Figure 12.** Examples of uniform scale change in difference images. Mid axial slices of: no scale change (left panel), repeat image scaled, prior to subtraction, by +1 % (middle panel), and by -1 % (right panel).

changes result from the shift in the cortical boundary. There are several alternately shaded bands corresponding to the cortical surface/CSF and CSF/dura interfaces. The innermost one corresponds to the cortical surface. For a uniform expansion the innermost one is a light shaded band. For contraction, the reverse, a dark shaded band, can be seen.

## 2.7. Visual Assessment

Two neuro-radiologists assessed both the unregistered images and the subtraction images corresponding to the two time points for each subject. For unregistered data the repeat and baseline scans were compared, for the registered data the corresponding difference images were assessed. Radiologists were blinded to both the subject and the method of image processing used. This was done by assigning the image identifiers with a random number generated with a widely available numerical algorithm (ran1).<sup>18</sup> So as eliminate any possible ambiguity with through plane misregistration the axial and coronal planes were viewed simultaneously with a 3D graphical tool.<sup>19</sup> Radiologists assessed overall change, degree of misregistration and the level of anatomical change. Structural change was only scored where there was a uniform band along an anatomical boundary in both viewing planes. A three point scale with: 0 (no change), 1 (probable change), 2 (definite change) and an optional +/- for each was used to score the assessments.

## 3. RESULTS

There were no assessment scores at the extremes ( 0- and 2+) so, to facilitate analysis, the scoring was converted into a 7 point scale with 1 (no change), 4 (probable change), 7 (definite change). The assessment scores for the two

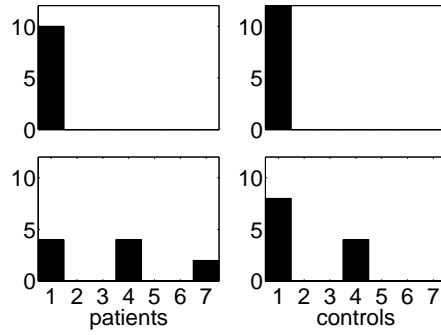


**Figure 13.** Histograms of assessed structural change for unregistered images. Observer A (top row), observer B (bottom row). The y axis of the histograms refers to the number of images and the x axis the assessed score (1 – 7).

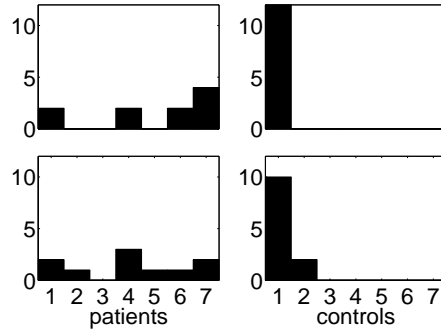


**Figure 14.** Histograms of assessed structural change for aligned and subtracted images. Observer A (top row), observer B (bottom row). The y axis of the histograms refers to the number of images and the x axis the assessed score (1 – 7).

radiologists and both time points were pooled, and the scores for the 3 processing methods are shown separately. Figure 13 shows graphically both observers’ assessed anatomical change from unregistered images, observer A (top row) and B (bottom row). Radiologist A (top row) did not record any structural change for any of the subjects. For radiologist B (bottom row) there was little difference between the patient and control groups. Figure 14 shows histograms of assessed structural change for aligned and subtracted images. Here there is a marked distinction between the groups, the patient group shows a range of scores while the control group shows all low scores. Figure 15 shows the assessments for scale corrected, aligned and subtracted images, the scores indicate a similar distinction between subject groups. Figure 16 shows example difference images for a subject from each of the two groups. The first pair of images (axial and coronal planes) are derived from a volunteer, within the brain region there are only noise-like patterns indicating little change. The second pair of images (axial and coronal planes) are derived from a GH patient and show anatomical change particularly around the lateral ventricles. Radiologists also recorded anatomical changes at sulci and the cortical surface for the GH patient group. The structural change was consistent with an increase in the brain/CSF ratio, the reverse of atrophic change.

### 3.1. Statistical Analysis

For small sample size (5 patients, 6 controls) we can not assume normally distributed scores. To analyse the significance of our results we must, therefore, use a non-parametric hypothesis test.<sup>20</sup> For qualitative scores the order and not the differences are meaningful so statistics based on rank are applicable. We assume that the subject groups are unmatched and therefore used the Wilcoxon rank sum test<sup>20</sup> with the null hypothesis there is no difference in assessed structural change between the two groups. The resultant p-value represents the probability of obtaining our observations given a true null hypothesis. We were also interested in the level of inter-observer agreement and decided that the Spearman rank correlation statistic,  $\rho$ , was the most appropriate statistic. Our results are

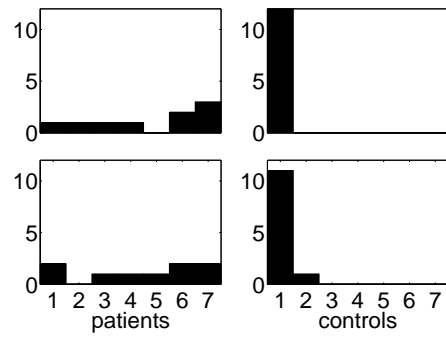


**Figure 15.** Histograms of assessed structural change for aligned, scale corrected and subtracted images. Observer A (top row), observer B (bottom row). The y axis of the histograms refers to the number of images and the x axis the assessed score (1 – 7).

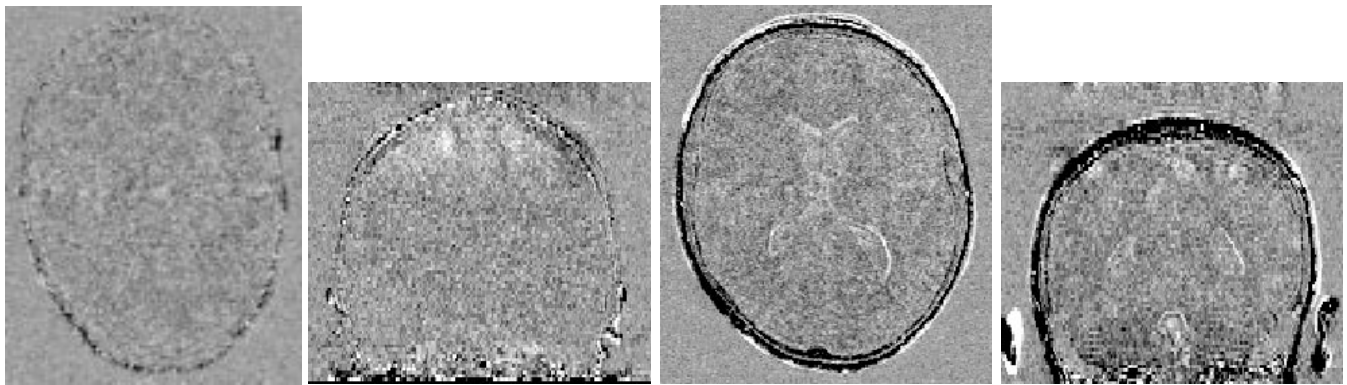


**Figure 16.** Mid axial and coronal planes through a difference image derived from a volunteer and showing no anatomical change (left). Corresponding planes through a difference image of a GH patient showing anatomical change (right). Note the white line around the ventricles and in some sulci indicating CSF volume reduction over time.

summarised by Table 2. A low p-value for the Wilcoxon rank sum test means that the null hypothesis is less likely to be true. The Table shows that discrimination between the groups, on the basis of structural change, is much greater for difference images compared with unregistered ones. For the unregistered images there was no agreement between observers (radiologist A did not score any change) whereas, for difference images there is very good agreement ( $\rho$  close to unity).

**Table 2.** Summary statistics on significance level and degree of inter-observer agreement for assessed structural change different methods of processing

method	Wilcoxon rank sum p-value	Spearman rank order $\rho$
unregistered images	0.14	-
aligned and subtracted images	$0.91 \times 10^{-3}$	0.9
aligned, scale corrected and subtracted images	$0.21 \times 10^{-3}$	0.89

#### 4. CONCLUSION AND DISCUSSION

Our results show that the detection of small anatomical change by visual assessment was significantly improved when aligned and subtracted images were used instead of unregistered images. There was a much greater level of inter-observer agreement of anatomical change for aligned and subtracted images than for unregistered images. We believe that accurate image alignment and training of radiologists in the interpretation of difference images contributed to the success of the method. Correction for intensity distortion would probably improve the results further.

#### ACKNOWLEDGEMENTS

We would like to thank Philips Medical Systems, EasyVision Advanced Development for funding this work, particular thanks go to Frans Gerritsen for his encouragement and constructive criticism. Thanks are also due to Jo Goodey, MR physicist, for scanning the volunteers and phantom. We are also grateful to D. Russel-Jones, endocrinologist, for the provision of clinical data.

#### REFERENCES

1. Hajnal J. V., Saeed N., Oatridge A., Williams E. J., Young I. R., and Bydder G. M., "Detection of Subtle Brain Changes Using Subvoxel Registration and Subtraction of Serial MR Images," *Journal of Computer Assisted Tomography* **19**(5), pp. 677–691, 1995.
2. De Boer H, Blok GJ, van der Veen VA, "Clinical aspects of growth hormone deficiency in adults.," *Endocrine Reviews* **16**, pp. 63–86, 1995.
3. Salomon F, Cuneo RD, Hesp R, Swensen PH, "The effects of treatment with recombinant human growth hormone on body composition and metabolism in adults with growth hormone deficiency," *New England Journal of Medicine* **321**, pp. 1797–1803, 1989.
4. McGauley GA, "Quality of life assessment before and after growth hormone treatment in adults with growth hormone deficiency," *Acta Paediatrica Scandinavica* **356 (Suppl)**, pp. 55–59, 1989.

5. Burman P, Broman JE, Hetta J, Wiklund I, Erfurth EM, Hagg E, Karlsson FA, "Quality of life in adults with growth hormone (GH) deficiency: response to treatment with recombinant human GH in a placebo-controlled 21-month trial," *Journal of Clinical Endocrinology and Metabolism* **80**, pp. 3585–3590, 1995.
6. Johansson JO, Larson G, Andersson M, Elmgren A, Hynsjo L, Lindahl A, Lundberg PA, Isaksson OG, Lindstedt S, Bengtsson BA, "Treatment of growth hormone-deficient adults with recombinant human growth hormone increases the concentration of growth hormone in the cerebrospinal fluid and affects neurotransmitters," *Neuroendocrinology* **61**, pp. 57–66, 1995.
7. Cranston I, Marsden P, Carroll P, Ward J, Sonksen P, Russell-Jones D., "Effect of growth hormone replacement on cerebral glucose metabolism and blood flow in adults with growth hormone deficiency - A preliminary report.," *Endocrinology and Metabolism*. **82**(6), pp. 2010–2013, 1997.
8. Freeborough P. A, Woods R.P, and Fox N. C., "Accurate Registration of Serial 3D MR Brain Images and its Application to Visualizing Change in Neurodegenerative Disorders," *Journal of Computer Assisted Tomography* **20**(6), pp. 1012–1022, 1996.
9. Lemieux L, Barker G, "Measurement of small inter-scan fluctuations in voxel dimensions in magnetic resonance images using registration," *Medical Physics* **25**(6), pp. 1049–1054, 1998.
10. Hajnal J. V., Saeed N., Soar E. J., Oatridge A., Young, I.R. and Bydder, G. M., "A Registration and Interpolation Procedure for Subvoxel Matching of Serially Acquired MR Images," *Journal Of Computer Assisted Tomography* **19**(2), pp. 289–296, 1995.
11. Studholme C, Hawkes DJ, Hill DLG, "A normalised entropy measure for multi-modality image alignment," in *Proceedings of Society of Photo-Optical Instrument Engineers (SPIE)*, vol. 3338, pp. 132–143, (San Diego), 1998.
12. Studholme, C. and Hill, D. L. G. and Hawkes, D. J., "An Overlap Invariant Entropy Measure of 3D Medical Image Alignment," *Pattern Recognition* **32**, pp. 71–86, Jan 1999.
13. Hill DLG, Maurer CR, Studholme C, Fitzpatrick JM, Hawkes DJ, "Correcting scaling errors in tomographic images using a nine degree of freedom registration algorithm," *Journal of Computer Assisted Tomography* **22**(2), pp. 317–323, 1998.
14. Bracewell R. N., *The Fourier Transform and its Applications*, McGraw-Hill, 1986. ISBN: 0-07-066454-4.
15. Freeborough PA, Fox NC, "Assessing Patterns and Rates of Brain Atrophy by Serial Magnetic Resonance Imaging: A Segmentation, Registration, Display and Quantification Procedure," in *Visualization in Biomedical Computing, S.P.I.E. Proc. vol. 1808, also Lecture Notes in Computer Science, 1996, Vol.1131*, pp. 419–429, 1996.
16. Lemieux L, Wiesmann et al, "The detection and significance of subtle changes in mixed-signal brain lesions by serial MRI scan matching and spatial normalisation," *Medical Image Analysis* **2**(3), pp. 227–242, 1998.
17. Sled JG, Zijdenbos AP, Evans AC, "A nonparametric method for automatic correction of intensity nonuniformity in MRI data," *IEEE Transactions on Medical Imaging* **17**(1), pp. 87–97, 1998.
18. Press W H, Teukolsky SA, Vetterling WT, Flannery BP, *Numerical Recipes in C. The art of Scientific Computing*, Cambridge University Press, Cambridge, 1992.
19. Studholme C, *Measures of 3D Medical Image Alignment*. PhD thesis, University of London, 1997.
20. Bland M, *An Introduction to Medical Statistics*, Oxford Medical Publications, 1995. ISBN: 0-19-262428-8.